Photodiode Amplifier with Transimpedance and Differential Stages for Automotive Visible Light Applications

Cătălin Beguni[1,2], Alin-Mihai Căilean[1,2], Sebastian-Andrei Avătămăniței[1,2] and Mihai Dimian[1,2]
[1]Department of Computers, Electronics and Automation, Stefan cel Mare University of Suceava, 720229 Suceava, Romania
[2]Integrated Center for research, development and innovation in Advanced Materials, Nanotechnologies, and Distributed Systems for fabrication and control, Stefan cel Mare University of Suceava, Suceava, Romania

***Abstract*— To address the most common issues found in automotive Visible Light Communication applications, a new photodiode amplifier based on an instrumentation amplifier is proposed. In order to improve the results, buffer stages have been replaced with transimpedance amplifiers providing the circuit with offset cancellation loops that enable the sensing of the DC output offset and with T-networks in the feedback path, that reduce the effect of parasitic capacitances. Thus, the resulted output signal will be ready for further processing in the analog-digital conversion (ADC) stage providing improved results in terms of parasitic light resilience and SNR.**

Keywords—automotive applications, common-mode rejection circuit, transimpedance amplifier, visible light communications.

I. INTRODUCTION

Visible Light Communications (VLC) are a relatively new technology that uses the visible light spectrum (380-780 nm) and the fast switching ability of solid-state lighting devices for lighting and wireless data transmission simultaneously [1], [2]. Due to the wide distribution of LED lighting sources which makes the VLC technology already half-implemented world-wide, numerous applications have already been found. Thus, the VLC technology is suitable for high data rate indoor applications [3], [4], high precision indoor localization [5], communication based vehicle safety applications [6], inter-vehicle distance determination [7], underwater communications [8], medical applications [9], while numerous other applications are continuously emerging. Nevertheless, in order to provide all these services, numerous challenges still need to be addressed. Many of these challenges are related to communication protocols, modulation and coding techniques, multi-user access and resource sharing, whereas some are still associated to the physical layer. Thus, the further improvement and development of high performances transimpedance circuits represents a hot research topic, as this stage has the highest importance in determining the overall performances of VLC systems [10]-[13]. So, in order to further expand all of the above mentioned applications, improved transimpedance circuits have to be developed continuously.

In this context, this paper proposes a new design of transimpendace circuit aimed for automotive applications [6]. The proposed design aims to provide high resilience to noise and high gain-bandwidth product (GBP). The paper describes all stages concerning the design and development of the proposed transimpedance circuit, providing this way a useful tool for such designs.

This work was supported by a grant of the Romanian Ministry of Research and Innovation, CCCDI - UEFISCDI, project number PN-III-P3-3.1-PM-RO-FR-2019-0282 / 21 BM/2019, within PNCDI III.

II. CONSIDERATIONS ON THE DESIGN REQUIREMENTS

A VLC receiver mainly consists of several main blocks: an optical collecting system with lens, optical filters and a photodetector, a preamplifier, a filtering stage, an amplifier stage along with clock and data recovery. Additionally, in some cases, biasing and compensation blocks may be necessary. The conversion of light into electric current can be done with various optoelectronic devices. However, photodiodes are singled out due to low cost, low switching time, good frequency response, linearity, low noise and high sensitivity reasons. However, the current generated by a photodiode is too small to be processed directly and so, it is required to convert it into a signal that is easier to process [13]. This conversion is done at the preamplifier stage and ideally, it should be done while limiting the amount of generated noise. As the preamplifier represents the main source of noise in the entire amplifier chain, its design will determine the sensitivity of the receiver.

There are three main possible implementations: with a low impedance amplifier, with a high impedance amplifier and with a transimpedance amplifier (TIA), each with its own advantages and disadvantages. The low-impedance amplifier has the widest input range, so a very good bandwidth can be achieved easily. However, this solution has as disadvantage a lower Signal-to-Noise Ratio (SNR), due to a small-value resistance at the input. In order to obtain a high SNR, a high-impedance amplifier can be used instead. This solution involves the usage of a high-value resistance, leading to an early saturation of the amplifier due to higher input levels. The transimpedance amplifier is a compromise between the first two solutions, as it is able to provide medium noise, high sensitivity and high bandwidth. These characteristics are achieved due to the fact that it typically has wider input current ranges than high-impedance amplifiers and better sensitivity than low-impedance amplifiers, one of the reasons being the negative feedback used in its design. Thus, considering that the

978-1-7281-6870-8/20/$31.00 ©2020 IEEE

transimpedance provides a fair tradeoff between gain-bandwidth product and noise, this solution is widely used in indoor [14]-[15] and outdoor [6], [7], [16], [17] VLC applications, being the most popular choice in this domain [18]. At the amplification stage, the signal is post-amplified for the data and clock recovery block. The post-amplifier does not add a significant noise in the system. Still, it is best to minimize the noise contributions anyway, especially the common-mode noise (from either the external electromagnetic signals or the switching power supply noise). One solution to address this issue is by choosing a differential amplifier for the post-amplification stage [19].

Considering the outdoor usage of the VLC system in automotive applications, and taking the strong parasitic sunlight into account [20], a compensation block can be added to attenuate the saturation when the receiver is subjected to direct sunlight.

To address the most common issues, an instrumentation amplifier is chosen as a foundation for this work. In order to improve the results, the instrumentation amplifier was modified with offset cancellation loops, based on two integrator circuits for sensing the DC output offset, T-networks being added in the feedback paths to reduce the effect of parasitic capacitances [21]. From this point, the output signal can be further process in the analog-digital conversion (ADC) stage until the data signal is reconstructed.

III. Considerations Regarding the Practical Design of the Transimpedance Circuit

The development of the transimpedance circuit begun with the aim of having a minimum of 1 mV_{pp} output for an input of 1 nA_{pp}, which means that a gain of around 1 MΩ is required. During the design stage, a classic transimpedance amplifier is considered as the starting point. Thus, the circuit illustrated in Fig. 1 is considered as a model for bandwidth analysis. The shunt resistance (R_{SH}) has usually a very high value, so it can be ignored. On the other hand, the input capacitance has a high impact on stability, bandwidth and noise [22]. The total input capacitance (C_S) is the sum of the photodiode capacitance (C_D), the common-mode capacitance of the amplifier (C_{icm}) and the differential capacitance of the amplifier (C_{id}). C_{icm} and C_{id} include both the board layout and the operational amplifier parasitic capacitance in accordance with eq. 1.

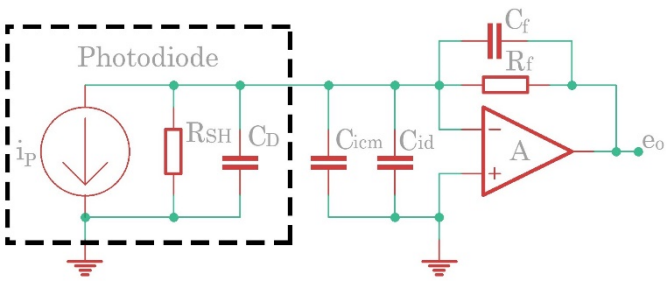

Fig. 1. Basic transimpedance circuit model.

$$C_S = C_D + C_{icm} + C_{id} \tag{1}$$

A. Stability Analysis

First, the non-infinite open-loop gain for a single pole op-amp model will be examined. The Bode plot illustrated in Fig. 2 shows the close-loop gain superimposed over the open-loop characteristic of the operational amplifier. This gain begins at 0 dB, and at the frequency f_z (determined by R_F and C_S) is starting to rise up. Uncompensated, the close-loop gain curve will rise and cross the operational amplifier open-loop gain A_{OL} at the frequency f_i. In order to avoid instability, a pole can be introduced at a frequency f_p with a compensation capacitor C_F in parallel with the feedback resistor R_F, which will limit the close-loop gain at $20\log(1+C_S/C_F)$. Imposing the condition $f_p \leq f_i$, the largest bandwidth will be obtained by lowering the C_F at the minimum value, which is given by eq. 2.

$$C_F = \sqrt{\frac{C_S}{2\pi R_F GBP}} \tag{2}$$

In order to maximize the bandwidth, the solution is to decrease the value of C_S and/or to increase the GBP. Lowering the value of C_S has the advantage of limiting the noise gain to a smaller value and to increase the zero response f_z to higher frequency. This means that an operational amplifier with low input capacitance and a photodiode with a low junction capacitance C_D must be considered. One adequate choice is the DET10A photodetector as it has a capacitance of only 10 pF. On the other hand, the sensitive area of the photodiode is also an important parameter, which in this case has only 0.8 mm^2. To increase the communication distance as required in automotive applications, the DET32A photodetector seems a more adequate choice as it has a capacitance of around 40 pF, but a larger sensitive area of 13 mm^2. Finally, because unity gain operational amplifier is not mandatory for a transimpedance application, a decompensated amplifier is a good choice, as it offers better voltage noise specifications and larger gain-bandwidth products. The OPA858 operational amplifier is an adequate choice in this case.

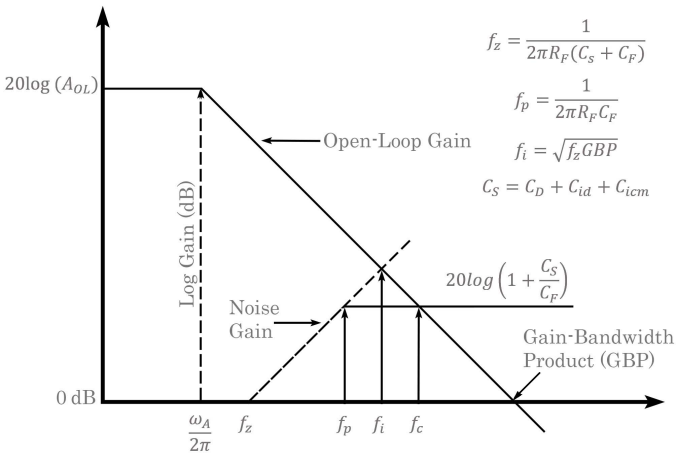

Fig. 2. Bode plot of the loop gain for the transimpedance operational amplifier configuration.

The gain is given by the relations 3 and 4.

$$V_O = -V^- A(s) \tag{3}$$

$$A(s) = \frac{A_{OL}\omega_A}{s+\omega_A} \tag{4}$$

Using Laplace transform function, the gain for the transimpedance operational amplifier is given by the relation 5.

$$\frac{V_O}{I_D} = \tag{5}$$

$$\frac{R_F \cdot \dfrac{A_{OL}\omega_A}{R_F(C_S+C_F)}}{s^2 + s\left(\omega_A\left(1+A_{OL}\dfrac{C_F}{C_S+C_F}\right)+\dfrac{1}{R_F(C_S+C_F)}\right)+\dfrac{\omega_A(A_{OL}+1)}{R_F(C_S+C_F)}}$$

The Gain-Bandwidth Product (GBP) is given by eq. 6.

$$\frac{A_{OL}\omega_A}{2\pi} = GBP \tag{6}$$

From here, the further calculation will lead to this relation:

$$\frac{V_O}{I_D} = R_F \cdot \frac{A_{OL}}{A_{OL}+1} \cdot \frac{\omega_O^2}{s^2 + s\dfrac{\omega_O}{Q} + \omega_O^2} \tag{7}$$

where:

$$\omega_O = \sqrt{\frac{\omega_A(A_{OL}+1)}{R_F(C_S+C_F)}} = f(2\pi) \tag{8}$$

$$Q = \frac{\sqrt{\dfrac{\omega_A(A_{OL}+1)}{R_F(C_S+C_F)}}}{\omega_A\left(1+A_{OL}\dfrac{C_F}{C_S+C_F}\right)+\dfrac{1}{R_F(C_S+C_F)}} \tag{9}$$

Using the following algebraic simplifications:

$$C_S \gg C_F \tag{10}$$

$$(A_{OL}+1)w_A \cong A_{OL}w_A = 2\pi \cdot GBP \tag{11}$$

$$\left(1+A_{OL}\frac{C_F}{C_F+C_s}\right) \cong A_{OL}\frac{C_F}{C_F+C_s} \tag{12}$$

these will lead to the eq. 13 and eq. 14.

$$f_i = \sqrt{f_z \cdot GBP} \tag{13}$$

$$Q = \frac{f_i}{f_z + f_c} \tag{14}$$

A. Bandwidth Considerations

An adequate VLC receiver must be able to work in an extended range of irradiance. The problem is that in outdoor conditions, the background light can have an irradiance going from a few μW/cm^2 up to more than 100,000 μW/cm^2. This parasitic light can heavily disturb the useful data. In these conditions, if the transimpedance circuit is too sensitive, this can lead to saturation. In [23], it was demonstrated that a logarithmic transimpedance circuit can compensate the background light up to 15,000 μW/cm^2. Nevertheless, the aim of this work is to further improve the transimpedance circuit with better components, additional compensation circuits for background light and also with common-mode noise reduction.

In Fig. 3, a topology which addresses the aforementioned problems is presented. Here, it should be underlined that intrinsic noise is at a higher level than that of a classical TIA. Even so, when coupled interference is predominant, the noise is better addressed with a differential configuration [24]. U1 and U3 are transimpedance amplifiers with resistive T-networks formed by R_1-R_2-R_3 and R_5-R_6-R_7 respectively, which can contribute to the increase of the bandwidth by reducing the effect of the parasitic capacitance. The outputs of these amplifiers are returned to the positive inputs through U2 and U4, which are in a classic Miller integrator topology. Their purpose here is to compensate the DC output offset appeared due to the sunlight or other external sources of light. Both outputs from the U1 and U3 are injected into a differential amplifier U5, in order to reject the common-mode interfering signals.

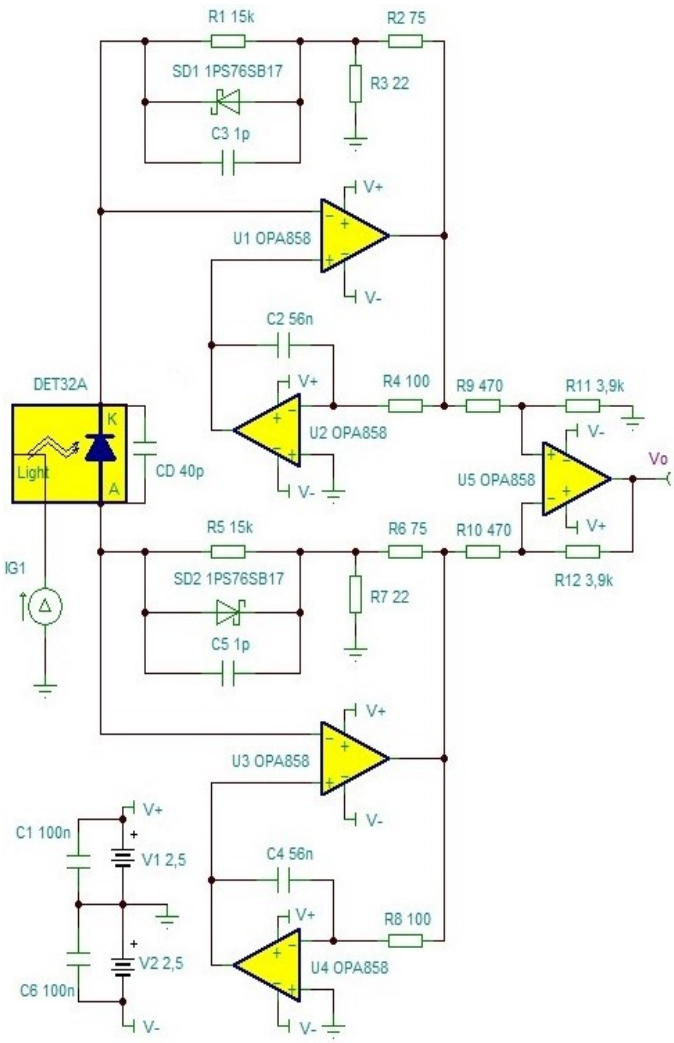

Fig. 3. Proposed transimpedance schematic.

IV. SIMULATIONS RESULTS

Before proceeding to the simulation section, some considerations are still required. As both branches of the differential amplifier are identical, only one of them is considered, while the results will be replicated for the other as well. So, U2 has a transfer function given by eq. 15.

$$H(s) = \frac{-1}{sR_4C_2} \tag{15}$$

This will return for U1 an output voltage over input current as follow:

$$\frac{V_{oU1}}{I_D} = \frac{R_{feq}}{(1+R_1C_3s)} \cdot \frac{R_3R_4C_2s}{R_2+R_3R_4C_2s} \tag{16}$$

where:

$$R_{feq} \cong R_1\left(1+\frac{R_2}{R_3}\right), \quad when \quad R_1 \gg R_2/R_3 \tag{17}$$

One can see that there are two poles at $-1/R_1C_3$ and at $-R_2/R_3R_4C_2$, and one zero at the origin. Then the lower 3 dB cutoff frequency f_L and the upper 3 dB cutoff frequency f_H are given by eq. 18 and 19.

$$f_H = \frac{R_2}{2\pi R_3R_4C_2} \tag{18}$$

$$f_L = \frac{1}{2\pi R_1C_3} \tag{19}$$

The communication frequency f_i is settled at 1 MHz which is high enough for the majority of the commercial vehicular LEDs. As the DET32A's photodiode has a rise time τ_r of 14 ns, significantly higher than that of an OPA858 (i.e. 0.3 ns), it should be verified if this could be an issue in choosing the proper f_H. Thus, by applying the following relation 20 [25]:

$$\tau_r \cong \frac{0.35}{f_{3dB}} \tag{20}$$

it is easy to determine that the chosen photodiode is not a limiting factor until $f_{3dB} \approx 20\ MHz$, and the margin is safe enough for a frequency $f_H = 10\ MHz$. It is best to have enough gain on this stage, but one must pay attention to the amplifier's saturation by ambient light. One can prevent this issue by inserting a diode SD1 in parallel with R_1 and choosing R_2-R_3 accordingly. 1PS76SB17 is an ultra-high-speed switching Schottky diode with a very low capacitance (0.8 pF) and a very low forward voltage (0.3 V) suitable in this case. The operational amplifier has a 2.5 V_{pp} output swing, so $R_2 = 22\ \Omega$ and $R_3 = 75\ \Omega$ can be used. In order to have a reasonable value for C_3 and a gain of around 50 kΩ for this stage, R_1 is settled at 15 kΩ. From eq. 18, one can now determine $C_3 = 1/2\pi R_1 f_H \leq 1/(2\pi R_1 \cdot 10\ MHz)$, which is around 1.06 pF, the maximum value for the chosen band. Taken eq. 2 into account, the stability condition imposes that C_3 must be greater or equal to 0.13 pF. A value of 1 pF is satisfying both conditions and it is setting the f_H to 10.6 MHz. As it is very much possible that the parasitic capacitance in the feedback path to be around this value, precaution must be taken in designing the PCB, because parasitic inductance and capacitance of the PCB traces can be a factor for instability at high frequencies.

As for the lower cutoff frequency f_L, it is enough to choose its value based on $f_L \leq 0.1f_i = 100\ kHz$ to avoid signal distortion. From eq. 19, it can be determined the time constant $R_4C_2 \geq 5.4\ \mu s$. For $R_4 = 100\ \Omega$ and $C_2 = 56$ nF, a $f_L = 96.9\ kHz$ value is obtained. The TINA simulation results showing the bode diagram are presented in Fig. 4.

As all the elements for one branch are now available, the gain of this stage can be determined based on eq. 16 and 17. Thus, the gain of this stage is 66 kΩ when the diode SD1 is not conducting, meaning that an output of at least 66 µV will be obtained for the minimum input current. The differential input for U5 will be in that case 132 µV, which establishes the necessary gain for this stage to around 8. As the values of R_9, R_{10} are established at 470 Ω, whereas R_{11}, R_{12} are equal to 3.9 kΩ, a total gain of around 1 MΩ is obtained.

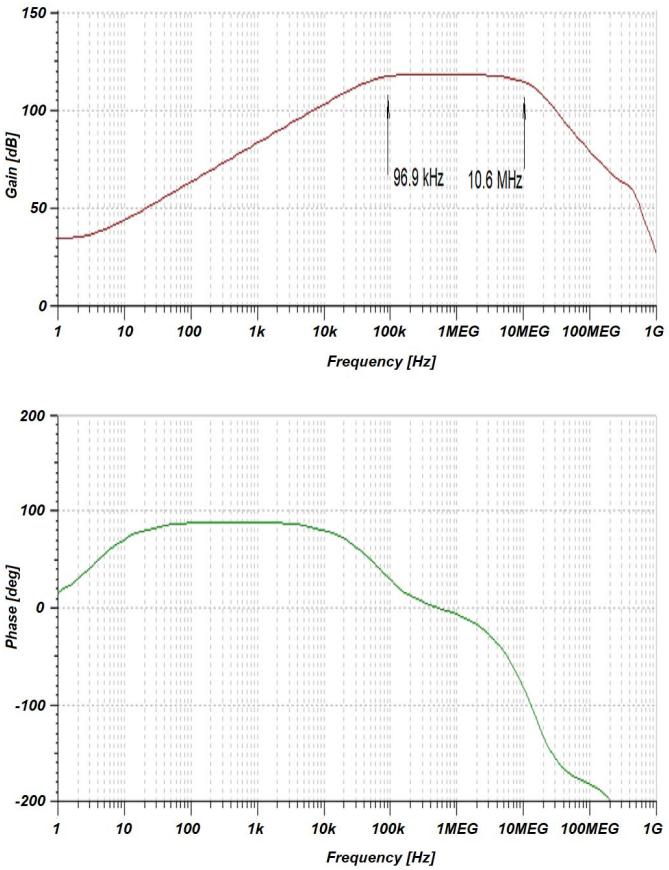

Fig. 4. Bode diagram simulation results.

V. DISCUSSION ON THE NOISE PERFORMANCES

The main sources of internal noise in a photodiode amplifier are shot noise, thermal noise, dark noise, flicker noise and amplifiers' current and voltage noises. The highest impact on the signal-to-noise ratio will be from the first stage, so

initially U1-U2 circuit will be considered using the noise model from Fig. 5 [26].

For a photodiode, the dominant source of noise is determined by the statistical uncertainty due to the discreet nature of the light and of the electrical current, called shot noise. This type of noise is usually found in semiconductor junctions, where the electrons pass the potential barrier in a discreet manner [24]. For a given photocurrent I_{PHD}, the noise contribution is given by eq. 21.

$$I_{shot} = \sqrt{2qI_{PHD}\Delta f} \tag{21}$$

For resistors, the dominant source of noise is the Nyquist-Johnson noise, also called thermal noise. The contribution in this case is given by the formula:

$$E_{thermal} = \sqrt{4kTR\Delta f} \tag{22}$$

For the FET operational amplifiers, the input current noises contribution can be ignored, as the main source of noise being the voltage ones. Apart from the noise gain, the signal gain is also required to estimate the SNR [19].

The amplifier's signal gain for U1 is determined from eq. 17. From the datasheet of the amplifier, it is easy to see that the flicker noise is relevant up until around 100 kHz and it is negligible in our frequency domain of interest (i.e. 1 MHz).

The Schottky diode will generate a lot less noise than the resistors in the feedback path, so it can be ignored as well.

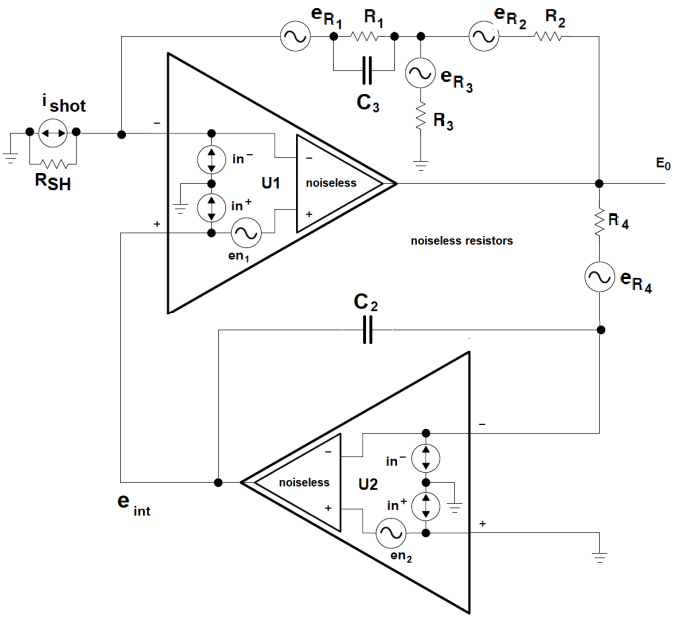

Figure 5. Noise analysis circuit.

From Fig. 5, there are the following noise contributors at the output:

$$E^2_{R_1out} = \left(1+\frac{R_2}{R_3}\right)^2 4kTR_1\Delta f \cong 4{,}000\,\text{nV}^2 \tag{23}$$

$$E^2_{R_3out} = \left(\frac{R_2}{R_3}\right)^2 4kTR_3\Delta f \cong 32\,\text{nV}^2 \tag{24}$$

$$E^2_{R_2out} = 4kTR_2\Delta f \cong 12\,\text{nV}^2 \tag{25}$$

$$E^2_{intR4} = \frac{kT}{\pi^2 R_4 C_2^2} \cong 0.0016\,\text{nV}^2 \tag{26}$$

One can see that the dominant source of noise here is the thermal noise of the feedback resistor. The noise of the photodiode will be amplified by the signal gain, so this cannot be improved. Regarding noises added by the integrator operational amplifier, these are low enough to be also ignored.

Finally, en_1 will be amplified by the noise gain, which is determined by the following relation 27 [27].

$$\frac{e_{noe}}{e_{ni}} = \left(1+\frac{R_2}{R_3}\right)\frac{1+R_{feq}(C_3+C_D)s}{1+R_{feq}C_3 s} \tag{27}$$

It can be seen that there is one zero at $-1/R_{feq}(C_3+C_D)$, and one pole at $-1/R_{feq}C_3$. So, we have $f_{pnoise} = 1/2\pi R_{feq}C_3$ and $f_{znoise} = 1/2\pi R_{feq}(C_3+C_D)$, which is the same as f_H.

The output noise is frequency dependent, with five distinct regions: region 1, dominated by flicker noise, region 2, with a direct transfer of the noise to the output, interrupted by the gain picking in region 3, followed by a plateau in region 4, and by an A_{OL} roll-off to infinite frequency [19]. Typically, this output noise component is dominated by the region 4 and 5. In this case, these values are given by eq. 28 and 29 leading in the end to relations 30 and 31.

$$E^2_{noe4} = \frac{(1+C_D)^2}{C_3^2}\left(\frac{C_3 GBP}{C_3+C_D} - \frac{1}{2\pi R_{feq}C_3}\right)\cdot e^2_{ni} \tag{28}$$

$$E^2_{noe5} = GBP\,\frac{C_3+C_D}{C_3}\,e^2_{ni} \tag{29}$$

$$E^2_{noe4} \cong 1{,}350\,\text{nV}^2 \tag{30}$$

$$E^2_{noe5} \cong 1{,}400\,\text{nV}^2 \tag{31}$$

For the final output noise, the result is given by eq. 32:

$$E_{noe} = \sqrt{2\frac{R_{11}}{R_9}\left(E^2_{R_1out} + E^2_{noe4} + E^2_{noe5}\right)} \cong 230\,\text{nV} \tag{32}$$

At the minimum input signal, V_{out} = 1 nA x 1 MΩ = 1 mV, the signal to noise ratio is given by 33.

$$SNR[dB] = 20\log\frac{V_{out}}{E_{noe}} \geq 72\,\text{dB} \tag{33}$$

The simulations provide encouraging evidence that the proposed circuit is able to cope with a parasitic light going up to 100,000 μW/cm² when the useful data signal is generating a photodiode current going up to 200 nA. Thus, this is a good

indicator that noise resilience can still be enhanced, contributing this way to vehicular communications compatible VLC systems. These results showed that this schematic is adequate for visible light communication in outdoor conditions, being able to cope with strong sunlight, to offer a good protection to noises and interferences, and with a high stability. On the downside, it should be mentioned that if it is to compare the proposed schematic with other proposals, this one has a higher complexity, which imposes a careful design for the PCB in order to eliminate the instability at high frequencies. Additionally, for an optimum common-mode performance, the circuit requires precision passive components' values. Hence, the overall cost is estimated to be higher.

VI. Conclusions

This paper provided an analytical evaluation based on simulations for a photodiode amplifier intended for VLC technology in automotive applications. The simulation results indicate that the proposed design has the potential to provide enhanced resilience to direct sunlight, good stability and high protection to noise. In the next step, hardware implementation and experimental evaluation of the design in a real case scenario are envisioned.

References

[1] M. Z. Chowdhury, M. T. Hossan, A. Islam and Y. M. Jang, "A Comparative Survey of Optical Wireless Technologies: Architectures and Applications," in *IEEE Access*, vol. 6, pp. 9819-9840, 2018. doi: 10.1109/ACCESS.2018.2792419

[2] L. E. M. Matheus, A. B. Vieira, L. F. M. Vieira, M. A. M. Vieira and O. Gnawali, "Visible Light Communication: Concepts, Applications and Challenges," in *IEEE Communications Surveys & Tutorials*, vol. 21, no. 4, pp. 3204-3237, Fourthquarter 2019. doi: 10.1109/COMST.2019.2913348

[3] D. Tsonev, S. Videv, H. Haas, "Towards a 100 Gb/s visible light wireless access network," *Optics Express,* vol. 23, no. 2, 1627–1637, 2015. doi: 10.1364/OE.23.001627

[4] R. Bian, I. Tavakkolnia and H. Haas, "15.73 Gb/s Visible Light Communication With Off-the-Shelf LEDs," in *Journal of Lightwave Technology*, vol. 37, no. 10, pp. 2418-2424, 15 May15, 2019. doi: 10.1109/JLT.2019.2906464

[5] Y. Zhuang *et al*., "A Survey of Positioning Systems Using Visible LED Lights," in *IEEE Communications Surveys & Tutorials*, vol. 20, no. 3, pp. 1963-1988, thirdquarter 2018. doi: 10.1109/COMST.2018.2806558

[6] A. Căilean and M. Dimian, "Current Challenges for Visible Light Communications Usage in Vehicle Applications: A Survey," in *IEEE Communications Surveys & Tutorials*, vol. 19, no. 4, pp. 2681-2703, Fourthquarter 2017. doi: 10.1109/COMST.2017.2706940

[7] B. Béchadergue, L. Chassagne and H. Guan, "Simultaneous Visible Light Communication and Distance Measurement Based on the Automotive Lighting," in *IEEE Transactions on Intelligent Vehicles*, vol. 4, no. 4, pp. 532-547, Dec. 2019. doi: 10.1109/TIV.2019.2938087

[8] M. Elamassie, F. Miramirkhani and M. Uysal, "Performance Characterization of Underwater Visible Light Communication," in *IEEE Transactions on Communications*, vol. 67, no. 1, pp. 543-552, Jan. 2019. doi: 10.1109/TCOMM.2018.2867498

[9] D. R. Dhatchayeny, A. Sewaiwar, S. V. Tiwari and Y. H. Chung, "Experimental Biomedical EEG Signal Transmission Using VLC," in *IEEE Sensors Journal*, vol. 15, no. 10, pp. 5386-5387, Oct. 2015. doi: 10.1109/JSEN.2015.2453200

[10] J. L. Cura and L. N. Alves, "Bandwidth improvements in transimpedance amplifiers for visible-light receiver front-ends," *2013 IEEE 20th International Conference on Electronics, Circuits, and Systems (ICECS)*, Abu Dhabi, 2013, pp. 831-834. doi: 10.1109/ICECS.2013.6815543

[11] R. Y. Chen and Z. Yang, "CMOS Transimpedance Amplifier for Gigabit-per-Second Optical Wireless Communications," in *IEEE Transactions on Circuits and Systems II: Express Briefs*, vol. 63, no. 5, pp. 418-422, May 2016. doi: 10.1109/TCSII.2015.2505264

[12] M. Basha, M. J. N. Sibley, P. J. Mather and A. Makama, "Design and Implementation of a Tuned Analog Front-End for Extending VLC Transmission Range," *2018 International Conference on Computing, Electronics & Communications Engineering (iCCECE)*, Southend, United Kingdom, 2018, pp. 173-177. doi: 10.1109/iCCECOME.2018.8658815

[13] C.R. Calvo, "A 2.5GHz Optoelectronic Amplifier in 0.18um CMOS", M.S. thesis, Worcester Polytechnic Institute, May 2003.

[14] A. Sewaiwar, P. P. Han and Y. H. Chung, "3-Gbit/s Indoor Visible Light Communications Using Optical Diversity Schemes," in *IEEE Photonics Journal*, vol. 7, no. 6, pp. 1-9, Dec. 2015, Art no. 7904609. doi: 10.1109/JPHOT.2015.2494498

[15] X. Li, B. Hussain, L. Wang, J. Jiang and C. P. Yue, "Design of a 2.2-mW 24-Mb/s CMOS VLC Receiver SoC With Ambient Light Rejection and Post-Equalization for Li-Fi Applications," in *Journal of Lightwave Technology*, vol. 36, no. 12, pp. 2366-2375, 15 June15, 2018. doi: 10.1109/JLT.2018.2813302

[16] A. Căilean, B. Cagneau, L. Chassagne, M. Dimian and V. Popa, "Novel Receiver Sensor for Visible Light Communications in Automotive Applications," in *IEEE Sensors Journal*, vol. 15, no. 8, pp. 4632-4639, Aug. 2015. doi: 10.1109/JSEN.2015.2425473

[17] M. Karbalayghareh, F. Miramirkhani, M. Safari and M. Uysal, "Vehicular Visible Light Communications with SPAD Receivers," *2019 IEEE Wireless Communications and Networking Conference (WCNC)*, Marrakesh, Morocco, 2019, pp. 1-5. doi: 10.1109/WCNC.2019.8885957

[18] O. Strobel, "Optical and Microwave Technologies for Telecommunication Networks", John Wiley & Sons, May 31, 2016.

[19] Graeme, Jerald G., "Photodiode Amplifiers: Op Amp Solutions", McGraw-Hill, 1996.

[20] M. S. Islim *et al*., "The Impact of Solar Irradiance on Visible Light Communications," in *Journal of Lightwave Technology*, vol. 36, no. 12, pp. 2376-2386, 15 June15, 2018. doi: 10.1109/JLT.2018.2813396

[21] P. Wright, K. B. Ozanyan, S. J. Carey and H. McCann, "Design of high-performance photodiode receivers for optical tomography," in *IEEE Sensors Journal*, vol. 5, no. 2, pp. 281-288, April 2005. doi: 10.1109/JSEN.2004.841869

[22] X. Ramus, "Transimpedance considerations for high-speed amplifiers," Application Report SBOA122. Texas Instruments, November 2009.

[23] S.A. Avătămăniței, A.M. Căilean, A. Done, M. Dimian, M. Prelipceanu, "Noise Resilient Outdoor Traffic Light Visible Light Communications System Based on Logarithmic Transimpedance Circuit: Experimental Demonstration of a 50 m Reliable Link in Direct Sun Exposure." Sensors, vol. 20, no. 3, pp. 909, 2020. doi: 10.3390/s20030909

[24] S. Franco, "Design with Operational Amplifiers and Analog Integrated Circuits", McGraw-Hill, 2002.

[25] "Relationship Between Rise Time and Bandwidth for a Low-Pass System" Thorlabs https://www.thorlabs.com/newgrouppage9.cfm?objectgroup_id=9817

[26] Noise Analysis in Operational Amplifier Circuits, Application Report SLVA043B, Texas Instruments, 2007.

[27] S. Zhang, C. Zhang, X. Pan, N. Song, "High-performance fully differential photodiode amplifier for miniature fiber-optic gyroscopes." in *Optics Express*. 27. 2125. doi: 10.1364/OE.27.002125.